Chapter - 4

Photoluminescence Studies of Europium Doped Strontium Gadolinium Niobate Oxide

4.1 Introduction

The ABX_3 structure, stand out by a wide margin, and pervoskite is far ahead of spinel as the single structure which, with skilled chemical manipulation, can produce an incredibly wide array of phases with totally different functions (Figure 4.1) [1].

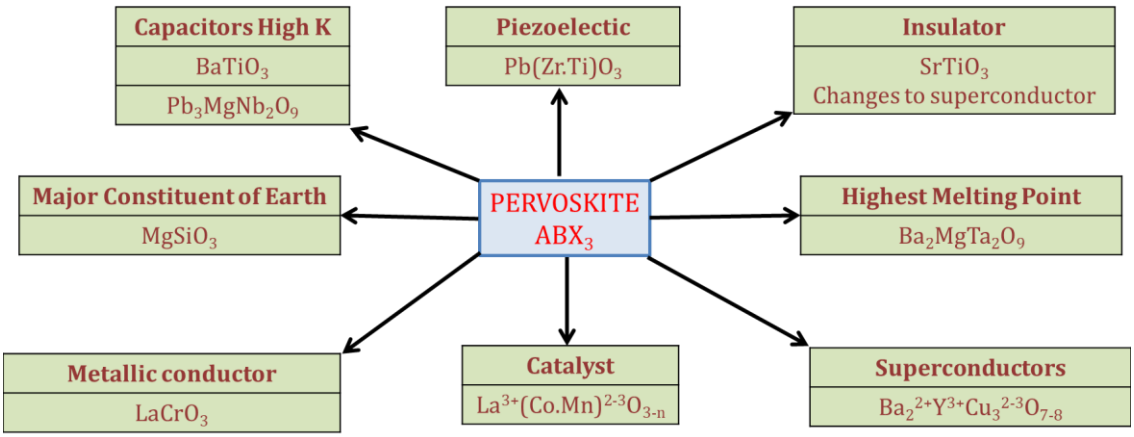

Figure 4.1 Pervoskite – the maximum multifunctional structure.

The emphasis on the importance of the structure-property relation is the key to the understanding of material science was a unique half-truth of the 1950s falsely imposed on the ages of students. In working to emphasize the importance of crystal or atomic structure as opposed hardly to gross composition, this facile expression led to the opposite error that the structure was a necessary predictor of properties. The pervoskite structure stands as an excellent example proving the error of this over-simplistic cliché [2].

The pervoskite structure is highly extensible in that it is capable of forming from an array of element sequences [2, 3]. Moreover, the versatility of this structure enables it to provide a wide range of deficiencies while maintaining structural stability [4 – 9]. Layered type heterostructures also form by pervoskite. In this kind of formation, pervoskite is interlayered with different compounds or structures [10]. One such example is the Ruddlesden-Popper phase [11 – 13], where layers of ABX_3 pervoskite and AX rock salt found to alternate through the material.

The versatility of the pervoskite structure is a result of its strength to distort. Divergence from the ideal cubic structure may occur due to ratios of non-ideal atomic radii, or electronic and magnetic effects, the structural changes characterized by rotations or distortions of the BZ_6 octahedra [14].

A Jahn-Teller distortion [15, 16] occurs in pervoskites if the B cation is an open shell transition metal. This kind of distortions is associated with increased separation in the energy between occupied and unoccupied d-orbital. For the cubic pervoskite structure, the regular BZ_6 octahedra result in d-orbitals splitting. This d-orbital split in three degenerate lower energies t_{2g} orbitals and two degenerate higher energy e_g orbitals. Distorting octahedra results in either the t_{2g} or e_g orbitals splitting. If either it partially occupied, the splitting would result in a stabilization of the system. Typically, two of the B-Z bonds in the octahedral complex elongate, and the other four shorten or two of the B-Z bonds contract and the other four elongate.

Pervoskites possess several useful properties, which lead them to use in a wide range of applications. Many ferroelectric pervoskites, like $BaTiO_3$, possess a high dielectric constant useful as capacitors. Ferroelectric capacitors are used in Ferroelectric RAM [17]. Ferroelectric pervoskite was also using as pyroelectric and piezoelectric. Thus, varying temperature and applied stress will induce a voltage. These make pervoskites such as $PbZr_{1-x}Ti_xO_3$ useful in sensor applications like pressure pads, microphones, and infrared sensors [2]. Pervoskite structure with Cuprates such as YBaCuO makes the majority of High-Temperature Superconductors (HTS) [18]. Magnetoresistance saw in some of the manganese-based pervoskites like $LnCaMnO_3$. The resistance of the material is varied by orders of magnitude in the presence of a magnetic field. The main possible application for magnetoresistance property is in hard drives, where the read heads currently make use of Tunnel Magnetoresistance [19]. Pervoskites like $LaMO_3$ are likely front-runners in electrochemical applications such as fuel cells [20], where the flexibility of the structure may aid ion transport.

4.2 Synthesis and Characterization

4.2.1 Synthesis

The Sr_2GdNbO_6: (X%) Eu (III) (Where X= 1, 2, 3, 4, 5) phosphor synthesized by solid-state synthesis method. The starting chemicals used for the synthesis of Sr_2GdNbO_6 are $SrCO_3$, Gd_2O_3, Nb_2O_5, and Eu_2O_3. These materials were intimately mixed in the stoichiometric ratio corresponding to the nominal composition of Eu (III) doped Sr_2GdNbO_6 and transferred it into alumina crucible. This mixture was heated at 1200^OC in a muffle furnace for 3 hours and then allowed it cool naturally to room

temperature. The obtained material crushed using mortar – pastel, the final product was obtained in powder form having white.

4.2.2 Characterization

XRD measurements of undoped and Eu(III) doped Sr_2GdNbO_6, were done using D8 Bruker advance X-Ray Diffractometer with the Cu Kα radiation with 8.05 keV energy, and 1.5406 Å wavelength (λ) at room temperature by step scanning with an angle range of $20° \leq 2\theta \leq 70°$ with increments of 0.02º. FTIR spectra of phosphors were, recorded using Jasco FTIR- 4100, spectrophotometer (Japan) by mixing phosphor with KBr through mortar - pestle in a ratio of 1:10. The PL of the samples examined using a Shimadzu spectrofluorophotometer (RF-5301 PC) at room temperature with a xenon lamp as an excitation source.

4.3 Results and Discussion

4.3.1 X-Ray Diffraction

Figure 4.2 shows the room temperature X-ray diffraction profile of Eu (III) doped Sr_2GdNbO_6. A good agreement between the observed and calculated inter planner spacing's (d-values) suggests that the compound crystallizes in monoclinic phase having $P2_1/n$ symmetry. The relative coordinates and occupancy of each site for Sr_2GdNbO_6 are shown in Table 4.1. The values for the bond distances of cations (relative to the oxygen anion) and occupancy were obtained from the Rietveld refinement. These are shown in Table 4.2. These diffraction lines are consistent and confirm the formation of a double pervoskite structure for all studied samples. The average crystallite size calculated using the Debye-Scherrer formula given in the literature [21] which is given as equation (4.1),

$$D = \frac{k.\lambda}{\beta.Cos\theta} \quad \text{----------} \quad (4.1)$$

Where, D is the average crystallite size, k is the constant equal to 0.94, λ is the wavelength of the X-rays equal to 0.1542 nm, θ is the Bragg angle and β is FWHM. All the reflection peaks of the X-ray profile indexed and lattice parameters are determined with the help of a standard computer program Powder-X.

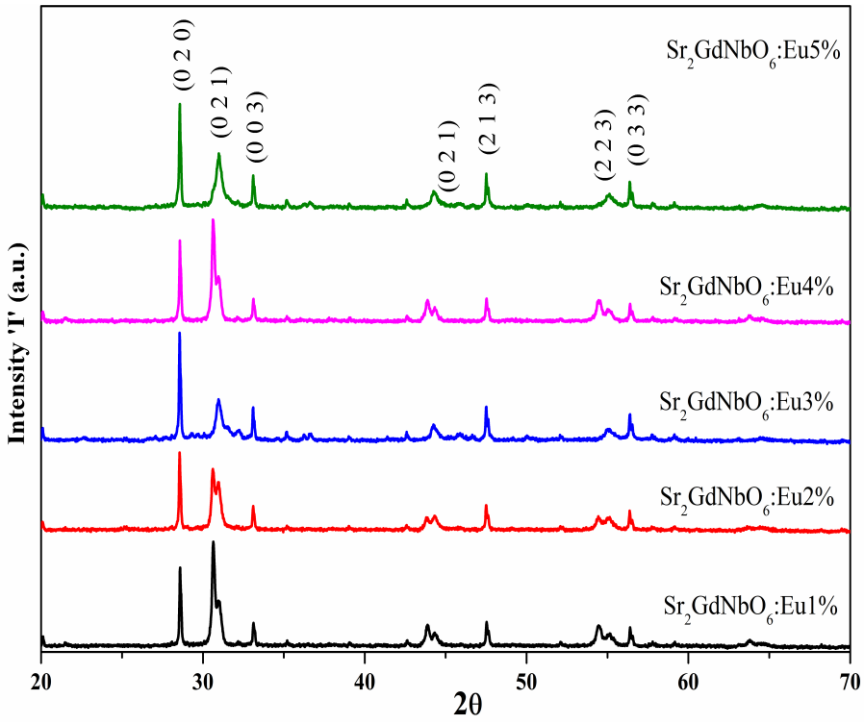

Figure 4.2 X-ray diffraction pattern of Eu(III) doped Sr_2GdNbO_6.

Atom	Site	*x*	*Y*	*z*
Sr	4e	0.5185	0.5543	0.2480
Gd	2c	0.0000	0.5000	0.0000
Nb	2d	0.5000	0.0000	0.0000
O	4e	0.2237	0.1880	-0.0463
O	4e	0.3163	0.7255	-0.0463
O	4e	0.4074	-0.0148	0.2306

Table 4.1 Structural parameters of Sr_2GdNbO_6 found by Rietveld analysis of XRD data.

All the reflection peaks of the X-ray profile indexed, and lattice parameters are determined with the help of a standard computer program Powder-X. In double pervoskite oxide, the study of distortion from the ideal cubic pervoskite structure is clear as the Sr_2GdNbO_6 complex pervoskite has the general formula $A_2BB'O_6$. The tolerance factor T_f [22] of the sample is calculated by using equation (4.2),

$$T_f = \frac{R_{Sr}+R_O}{\sqrt{2}\left(\frac{R_{Gd}+R_{Nb}}{2}+R_O\right)} \quad \text{---------- (4.2)}$$

Where, R_{Ba}, R_{Ce}, R_{Nb} and R_O are the ionic radii of Sr, Gd, Nb and O respectively [23]. By the geometry of crystal, the ideal cubic structure should have $T_f = 1$, whereas it will

be monoclinic structure for values of $T_f < 1$ and it following the SPuDs prediction [24]**.** The value of tolerance factor for Sr_2GdNbO_6 was found to be approximately 0.9218, which suggests that sample under study has the monoclinic structure.

Cation	Anion & Multi.	Distance (Å)	Occupancy
Gd (2c)	O (4e) X 2	2.2872	1.00
Gd (2c)	O (4e) X 2	2.2891	1.00
Gd (2c)	O (4e) X 2	2.2881	1.00
Nb (2d)	O (4e) X 2	1.9776	1.00
Nb (2d)	O (4e) X 2	1.9793	1.00
Nb (2d)	O (4e) X 2	1.9777	1.00
Sr (4e)	O (4e) X 1	3.6747	1.00
Sr (4e)	O (4e) X 1	2.9365	1.00
Sr (4e)	O (4e) X 1	2.7027	1.00
Sr (4e)	O (4e) X 1	2.5186	1.00
Sr (4e)	O (4e) X 1	2.8788	1.00
Sr (4e)	O (4e) X 1	3.6833	1.00
Sr (4e)	O (4e) X 1	2.5354	1.00
Sr (4e)	O (4e) X 1	2.7426	1.00
Sr (4e)	O (4e) X 1	3.3278	1.00
Sr (4e)	O (4e) X 1	2.4867	1.00
Sr (4e)	O (4e) X 1	3.4425	1.00
Sr (4e)	O (4e) X 1	2.6414	1.00

Table 4.2 Inter-atomic distance and occupancy calculated through Rietveld refinement of experimental data.

Williomson – Hall Plot

Scherrer formula examines only the effect of crystallite size on the XRD peak broadening, but it doesn't give any information about the microstructures of the lattice about the intrinsic strain, which gets improved in the nanocrystals due to the point defect, grain boundary, triple junction and stacking faults [25].

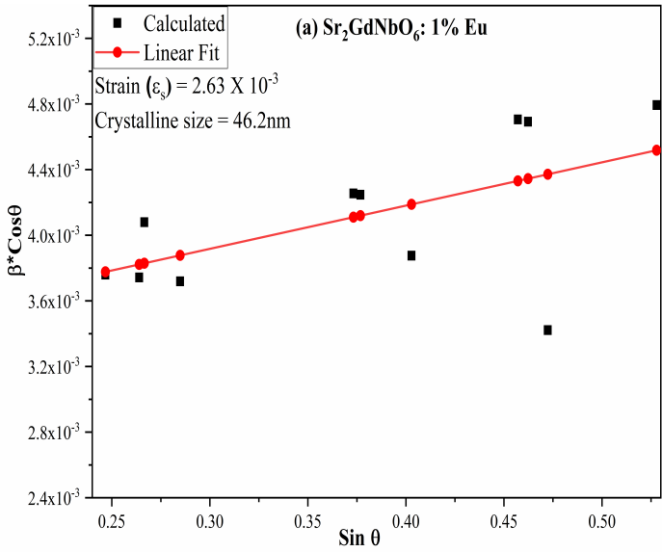
Calculated
Linear Fit
(a) Sr2GdNbO6: 1% Eu
Strain (εs) = 2.63 X 10-3
Crystalline size = 46.2nm
β*Cosθ
Sin θ

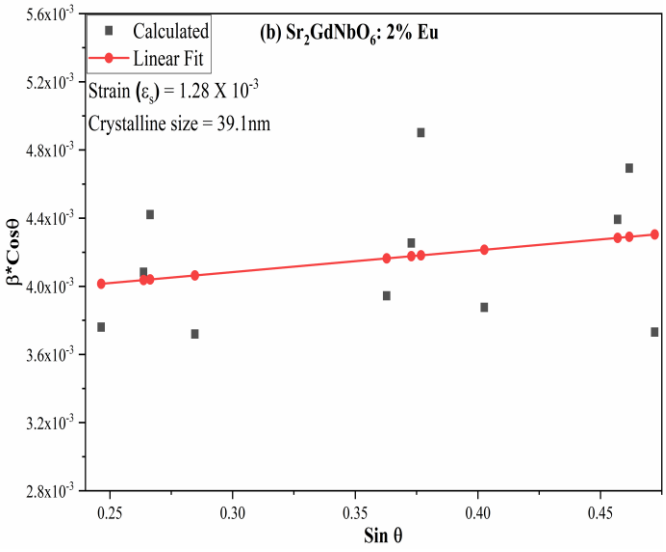
Calculated
Linear Fit
(b) Sr2GdNbO6: 2% Eu
Strain (εs) = 1.28 X 10-3
Crystalline size = 39.1nm
β*Cosθ
Sin θ

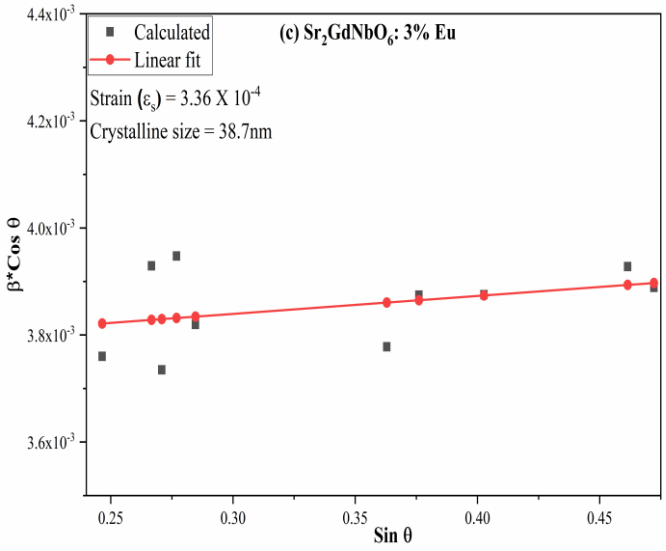
Calculated
Linear fit
(c) Sr2GdNbO6: 3% Eu
Strain (εs) = 3.36 X 10-4
Crystalline size = 38.7nm
β*Cos θ
Sin θ

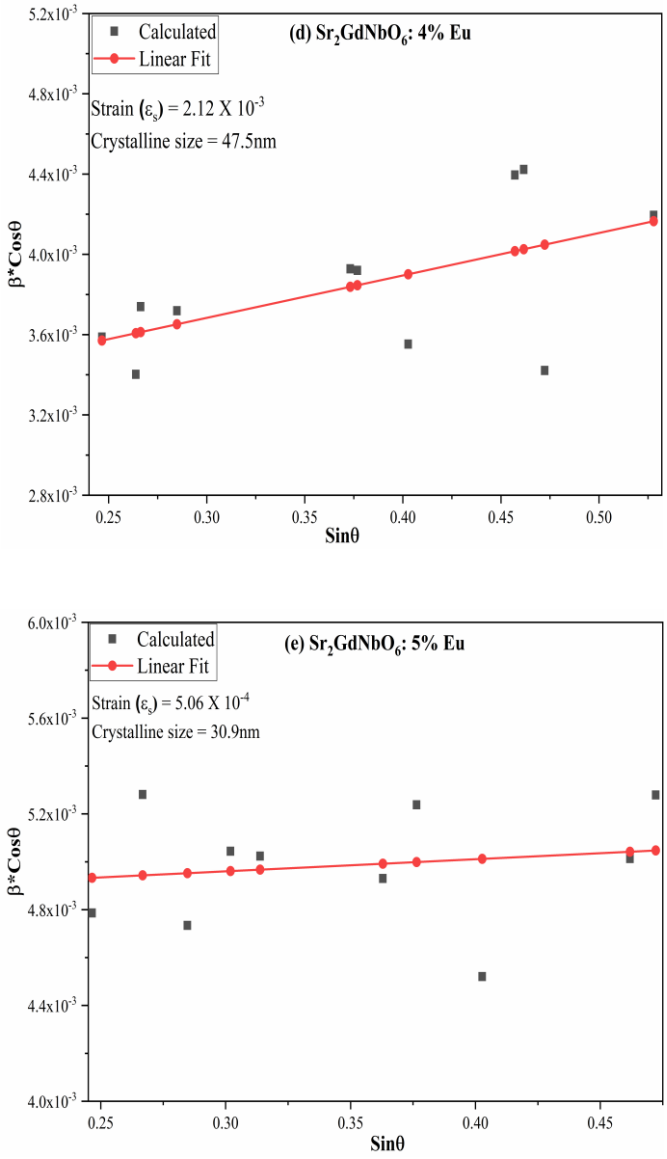

Figure 4.3(a–e) Williomson-Hall plot of Eu(III) doped Sr_2GdNbO_6.

There are many methods such as the Williamson Hall method, Warren-Averbach method, etc., which considers the effect of the strain-induced XRD peak broadening and can use for the calculation of the intrinsic strain along with the particle size. Among these methods, the Williamson–Hall (W–H) method is a very easy and simplified one [25 – 28].

Figure 4.3 (a-e) shows W-H plot of Eu (III) doped Sr_2GdNbO_6. The broadening effect of XRD peaks reflects the nanocrystalline nature of the resulting Eu(III) doped Sr_2GdNbO_6 samples. Since the effective XRD peak broadening can caused by lattice strain and small crystallite size, these two effects have to be distinguished. This can be

calculated by plotting β cosθ versus sinθ in the following relation (equation 4.3) (Williamson–Hall plot) [21],

$$\beta_{hkl} * cos\theta_{hkl} = \left(\frac{k\lambda}{D}\right) + \varepsilon * sin\theta_{hkl} \text{ ---------- (4.3)}$$

The crystallite size and strain of Eu(III) doped Sr_2GdNbO_6 estimated from the intercept and slope are listed in Table 4.3.

Sample		**Sr_2GdNbO_6: Eu^{3+} (1 %)**	**Sr_2GdNbO_6: Eu^{3+} (2 %)**	**Sr_2GdNbO_6: Eu^{3+} (3 %)**	**Sr_2GdNbO_6: Eu^{3+} (4 %)**	**Sr_2GdNbO_6: Eu^{3+} (5 %)**
Structure		Monoclinic	Monoclinic	Monoclinic	Monoclinic	Monoclinic
Space Group		$P2_1/n$	$P2_1/n$	$P2_1/n$	$P2_1/n$	$P2_1/n$
Cell Parameters	**a(Å)**	6.0120	5.9889	5.9846	6.0245	6.0025
	b(Å)	6.1402	6.1435	6.2940	6.2745	6.1203
	c(Å)	8.0958	8.0985	8.1035	8.0992	8.1306
	β	90.080	89.920	89.950	90.1	89.98
Volume $(Å)^3$		298.855	297.966	305.235	306.155	298.694
Average Crystallite Size (nm)	**Scherrer Method**	35.55	35.1	34.2	37.9	29.1
	W-H Plot	46.2	39.1	38.7	47.5	30.9
Strain (ε)		2.63×10^{-3}	1.28×10^{-3}	3.36×10^{-4}	2.12×10^{-3}	5.06×10^{-4}

Table 4.3 Summary of cell parameter, volume and crystalline size of Eu(III) doped Sr_2GdNbO_6.

4.3.2 FTIR (Fourier Transform Infrared Spectrometry)

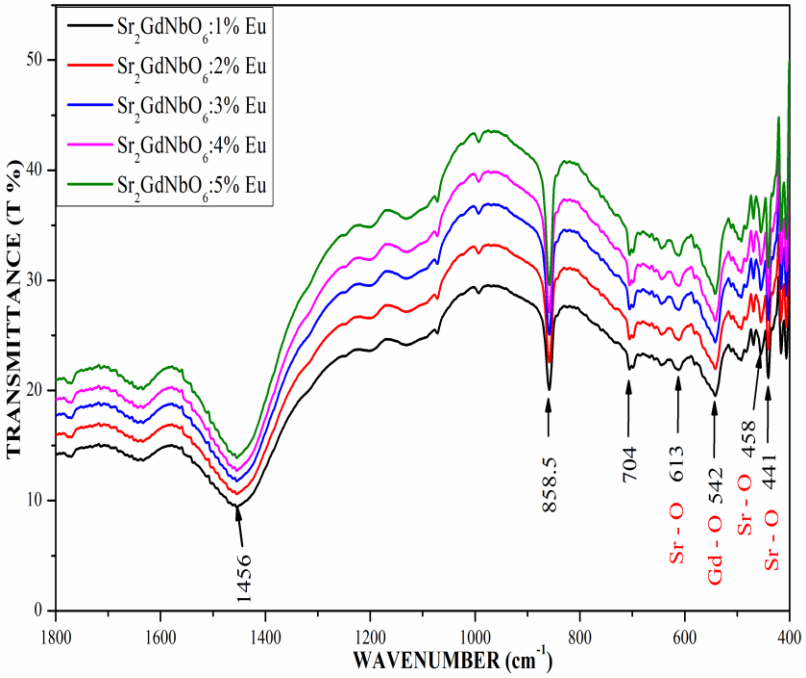

Figure 4.4 FTIR spectra of Eu(III) doped Sr_2GdNbO_6.

In order to determine the atomic bonds in a molecule FTIR analysis was carried out. In Figure 4.4 FTIR spectra of Sr_2GdNbO_6 has shown with a range of 400 cm^{-1} to 1800 cm^{-1} wavenumber. The FTIR spectrum of Sr_2GdNbO_6 shows some well-defined bands in the figure 4.4. It is in good accordance with what orderly found for a pervoskite type structure following group theory predictions [29]. In pervoskite-type material, significant vibrational couplings may expect between the different coordination polyhedral compounds. The observed shoulder peak at 704 cm^{-1} recommends the overlapping of Sr_2O_6 and NbO_6 stretching bands with the displacement toward higher frequencies of the NbO_6 bands [30]. Several pervoskite-type oxides and especially in the niobium containing compounds corner-shared and edge-shared octahedra may present [31, 32]. Corner-shared and edge-shared octahedra are predominant in niobium-oxygen polyhedral compounds where edge-shared octahedra exhibit large distortions compared to corner-shared octahedra which appearing in significant alterations in Nb-O bond lengths. For the edge-shared octahedra the Nb-O bond length varies from 1.7 to 2.3 Å, whereas in corner-shared octahedra Nb-O bond lengths ranges from 1.8 to 2.1 Å [33, 34].

The bands at 542 cm^{-1} are assigned to the Gd-O vibration [35 – 37]. For the end edge-shared NbO_6 octahedra, the symmetric stretching vibrations are observed in 850-

1000 cm^{-1} wavenumber range. Whereas in the case of corner shared octahedra, these vibrations in 750cm^{-1} to 850 cm^{-1} region [38, 39]. The identical spectral pattern, with four well-defined IR bands in the 400-750 cm^{-1} range, had been found in a great number of $A_2BB'O_6$ pervoskite type materials, and they were assigned in the same way [38 –42]. In the present study, the symmetric stretching vibrations from 838.8 cm^{-1} completely support the possible presence of edge-connected Nb-O octahedra.

4.3.3 Photoluminescence

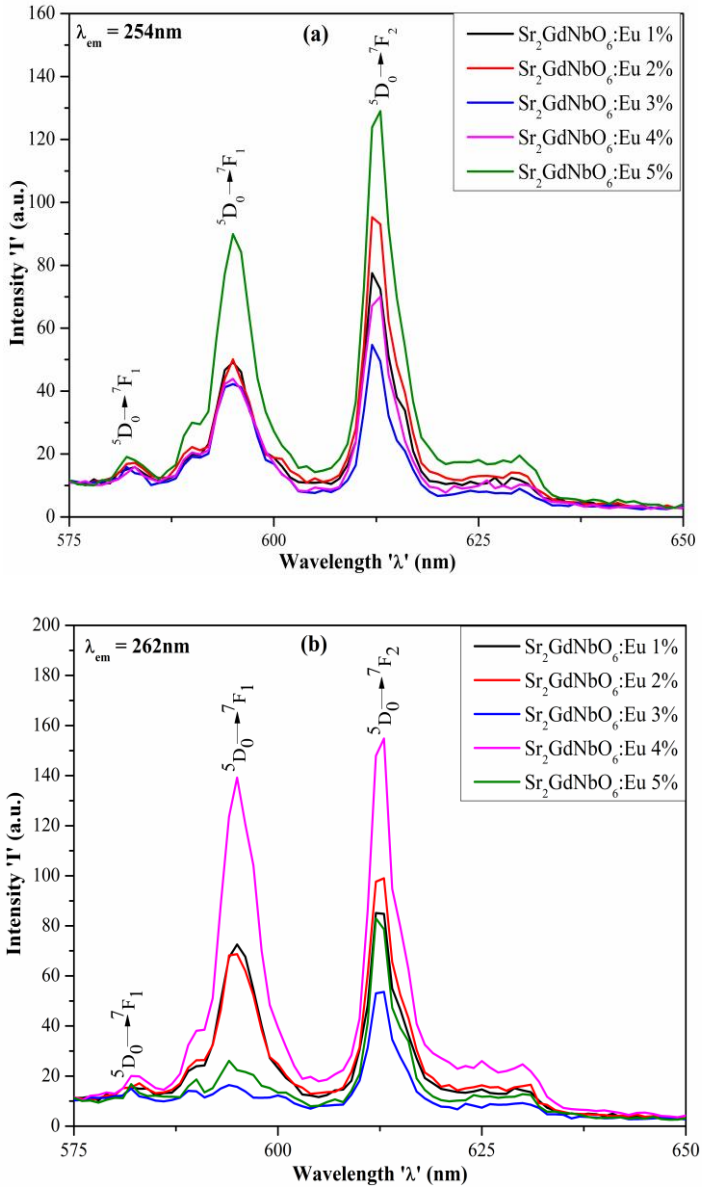

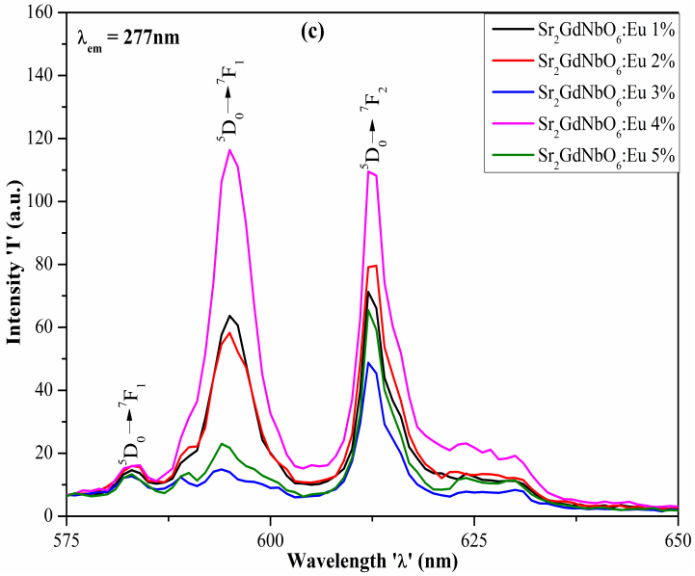

Figure 4.5 Photoluminescence emission spectra of Eu(III) doped Sr_2GdNbO_6.
(a) excitation wavelength 254nm, (b) excitation wavelength 262nm, and (c) excitation wavelength 277nm.

Figure 4.5 (a-c) presents room temperature emission spectra of Eu(III) doped Sr_2GdNbO_6 phosphors excited at 254nm, 262nm, and 277nm. Here, the concentration of europium varied from 1 to 5 mol percentage. The Eu(III) doped Sr_2GdNbO_6 samples exhibit three visible emission bands around 582, 596, and 613 nm. These assigned to the magnetic dipole (MD) and electric dipole (ED) transitions of europium $^5D_0 \rightarrow {}^7F_1$, $^5D_0$ - $^7F_2$. The emission of Eu(III) has assigned to transition from the $^5D_1$ and $^5D_0$ levels to the ^7F_J (J = 0 – 6) levels [43]. The photoluminescence emission peaks in 580–600 nm range are due to the magnetic dipole transition of $^5D_0 \rightarrow {}^7F_1$, which is lower than that of the intensity of the $^5D_0 \rightarrow {}^7F_2$ transition. This transition confirms that the Eu(III) ions situated at the non-inversion symmetric sites [44, 45]. It is worthwhile to note that all emission spectra show an intense emission peak at around 613nm in the red region, which attributed to the $^5D_0 \rightarrow {}^7F_2$ transition. This red emission from the Eu(III) luminescence center has a better perception of the human eye. However, an admixture of odd-parity electronic configuration to the pure 4f level will allow the electric dipole transitions partially, and their probability of occurrence is much higher than the chance of parity-allowed magnetic dipole (MD) ($^5D_0 \rightarrow {}^7F_1$) transition. The site symmetry of Eu^{3+} ion in the host lattice can be predicted by asymmetry ratio, which can be defined by equation (4.4),

$$asymmetry - ratio = \frac{I(5D_0 \rightarrow 7F_2)}{I(5D_0 \rightarrow 7F_1)} \text{ ---------- (4.4)}$$

Where, I($^5D_0 \rightarrow {}^7F_2$) and I($^5D_0 \rightarrow {}^7F_1$) are the intensities of electric dipole and magnetic dipole transition peaks, respectively. If the asymmetry ratio is more than one, then Eu(III) substituted at the non-centrosymmetric site. For the asymmetric proportion less than 1, Eu(III) placed at a centrosymmetric position in the host lattice. Here, the asymmetry ratio found to be more than 1, so the phosphor shows that Eu(III) placed at A site in the host lattice and is in good agreement with the presently reports [46 – 51]. It could understand that the substitution of Eu(III) at Sr(II) site in Sr_2GdNbO_6 is followed by Sr(II) ion vacancy due to charge imbalance and lattice strain due to different ionic radius. These defects in lattice reduce the local site symmetry at the Eu(III) site and act as a luminescence quenching center.

Sr. No.	Sample	Asymmetry Ratio		
		at 254nm	**at 262nm**	**at 277nm**
1	Sr_2GdNbO_6: Eu(1%)	1.6	1.18	1.11
2	Sr_2GdNbO_6: Eu(2%)	1.9	1.45	1.34
3	Sr_2GdNbO_6: Eu(3%)	1.3	3.2	3.46
4	Sr_2GdNbO_6: Eu(4%)	1.6	1.11	0.95
5	Sr_2GdNbO_6: Eu(5%)	1.44	3.24	2.78

Table 4.4 Asymmetric ratio of Eu(III) doped Sr_2GdNbO_6 at 254nm, 265nm and 277nm emission spectra.

CIE (Commission International del'éclairage)

The emission spectra of Eu(III) doped Sr_2GdNbO_6 examined, and the chromaticity color coordinates of all samples calculated. The Commission International del'éclairage (CIE) 1931 diagram is depicted in Figure 4.6 (a-c). With the increasing europium concentration, the color tone of the emanating light shifts from orange to the red region. The results also show that the Eu(III) doped phosphors herein reported extended further to the latitude of the orange-red tenability region after compared to reported results [52 – 55].

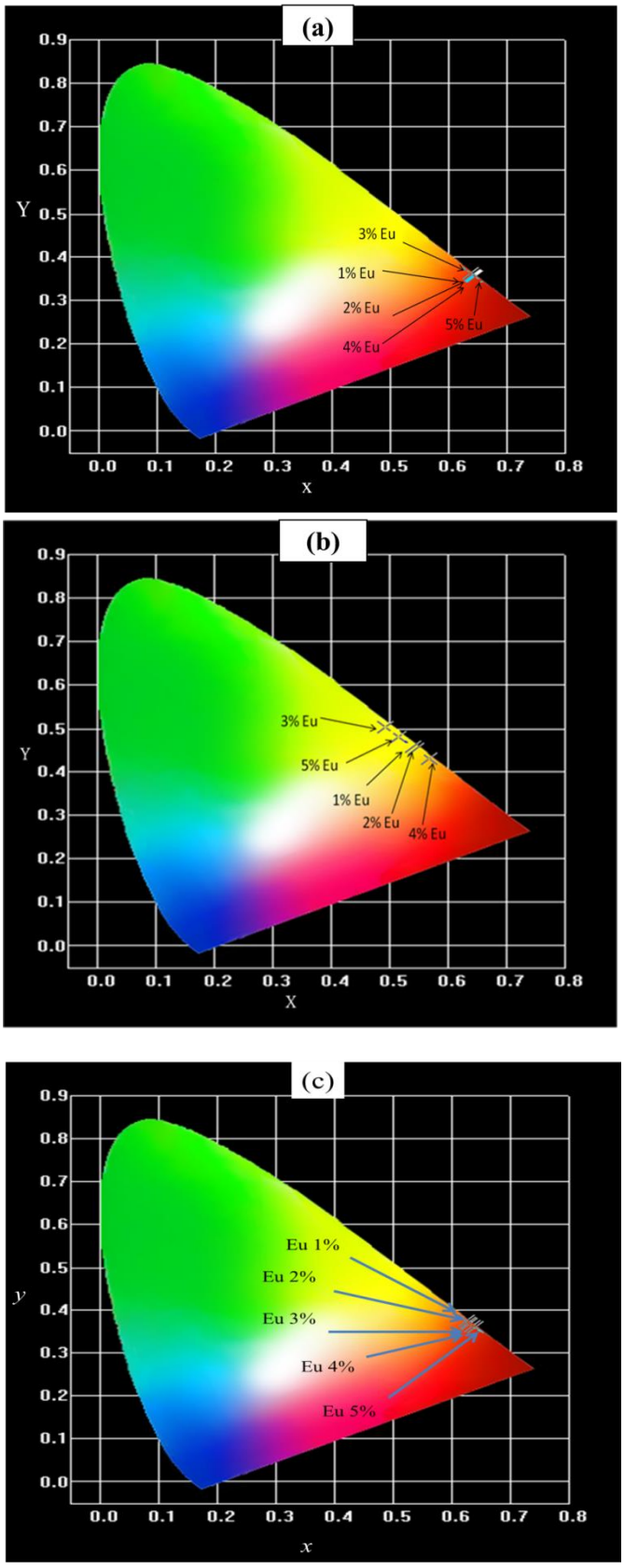

Figure 4.6 (a-c) CIE diagram of Eu(III) doped Sr_2GdNbO_6.

It is good to point out that the incorporation of the emission color corresponding to coordinate points (Figure 4.6 (a-c)) yields a mixture of light with color in the orange-red region possess glow correlated color temperature, i.e., CCT in the 1700K – 2500K range. We have admittedly simulated the generation flow CCT for red-light using xenon lamp, and the phosphors herein reported [56 – 58]. Table-4.5 shows the CIE1931 coordinates and associated correlated color temperature of the overall emission.

Sr. No.	Sample	254 nm				262 nm				277 nm			
		x	Y	CCT		x	y	CCT		x	y	CCT	
				Calcu.	Software			Calcu.	Software			Calcu.	Software
1	Sr_2GdNbO_6: Eu (2%)	0.642	0.357	2297.096	2306	0.541	0.457	2149.956	2168	0.626	0.374	1751.782	1921
2	Sr_2GdNbO_6: Eu (3%)	0.645	0.354	2436.266	2403	0.545	0.453	2093.64	2115	0.628	0.371	1786.208	1966
3	Sr_2GdNbO_6: Eu (4%)	0.637	0.362	2103.525	2164	0.538	0.446	2104.95	2125	0.631	0.368	1831.621	2024
4	Sr_2GdNbO_6: Eu (5%)	0.641	0.358	2232.48	2276	0.567	0.431	1823.434	1864	0.634	0.362	1919.988	2136
5	Sr_2GdNbO_6: Eu (1%)	0.643	0.356	2382.59	2337	0.516	0.481	2528.094	2534	0.639	0.359	2000.372	2236

Table 4.5 CIE 1931 coordinates and CCT of the emissions under (254nm, 262nm, and 466nm) xenon lamp excitation.

4.4. Outcome

Eu^{3+} doped Strontium Gadolinium Niobate (SGN) oxide has been synthesizing by the solid state reaction method. The X-ray diffraction measurement of Strontium Gadolinium Niobate (SGN) oxide revels that phosphor has a monoclinic phase with space group $P2_1/n$ (# 014). Prepared pervoskite phosphor is nanocrystalline measured through Scherrer's method and Williamson-hall plot method. Shifting in XRD patterns is also reflected in the Williamson–Hall plot, which occurred due to the highly strained and distorted environment in the Sr_2GdNbO_6 lattice**.**

FTIR of Sr_2GdNbO_6 gives information that phosphor has a nano-size pervoskite structure with an edge-connected Nb-O octahedral. The bands at 542 cm^{-1} are assigned to the Gd-O vibration. The observed shoulder peak at 704 cm^{-1} recommends the overlapping of Sr_2O_6 and NbO_6 stretching bands with the displacement toward higher frequencies of the NbO_6 bands. The symmetric stretching vibrations from 838.8 cm^{-1} completely support the possible presence of edge-connected Nb-O octahedra.

Room temperature photoluminescence spectra of phosphor recorded using a Xenon lamp as a source. A Photoluminescence study of Eu^{3+} doped Sr_2GdNbO_6 phosphor shows that Eu^{3+} substituted at A-site at 254nm, 262nm and 277nm. Photoluminescence spectra of phosphor show high-intensity peaks at 590nm and 610nm due to $^5D_0 \rightarrow {}^7F_1$ and $^5D_0 \rightarrow {}^7F_2$ transitions of Eu^{3+} ions. The substitution of Eu^{3+} at Sr^{2+} site in Sr_2GdNbO_6 is followed by Sr^{2+} ion vacancy due to charge imbalance and lattice strain due to different ionic radius. With the increasing europium concentration, the colour tone of the emanating light shifts from orange to the red region. The emission colour corresponding to coordinate points yields a mixture of light with colour in the orange-red region possess glow correlated colour temperature, i.e., CCT in the 1700K – 2500K range.

References

[1] O. Muller and R. Roy, *The Major Ternary Structural Families*. Berlin, Heidelberg: Springer Berlin Heidelberg, 1974.

[2] A. S. Bhalla, R. Guo, and R. Roy, "The pervoskite structure—a review of its role in ceramic science and technology," *Mater. Res. Innov.*, vol. 4, no. 1, pp. 3–26, Nov. 2000.

[3] C. Li, K. C. K. Soh, and P. Wu, "Formability of ABO3 pervoskites," *J. Alloys Compd.*, vol. 372, no. 1–2, pp. 40–48, Jun. 2004.

[4] M. Islam, "Computer modelling of defects and transport in pervoskite oxides," *Solid State Ionics*, vol. 154–155, pp. 75–85, Dec. 2002.

[5] T. Ishihara, H. Matsuda, and Y. Takita, "Doped LaGaO3 Pervoskite Type Oxide as a New Oxide Ionic Conductor," *J. Am. Chem. Soc.*, vol. 116, no. 9, pp. 3801–3803, May 1994.

[6] M. V. Raymond and D. M. Smyth, "Defects and charge transport in pervoskite ferroelectrics," *J. Phys. Chem. Solids*, vol. 57, no. 10, pp. 1507–1511, Oct. 1996.

[7] M. Alfredsson *et al.*, "Dopant control over the crystal morphology of ceramic materials," *Surf. Sci.*, vol. 601, no. 21, pp. 4793–4800, Nov. 2007.

[8] K. Huang, R. S. Tichy, and J. B. Goodenough, "Superior Pervoskite Oxide-Ion Conductor; Strontium- and Magnesium-Doped LaGaO3: I, Phase Relationships and Electrical Properties," *J. Am. Ceram. Soc.*, vol. 81, no. 10, pp. 2565–2575, Jan. 2005.

[9] Y. F. Zhukovskii, E. A. Kotomin, S. Piskunov, and D. E. Ellis, "A comparative ab initio study of bulk and surface oxygen vacancies in PbTiO3, PbZrO3 and SrTiO3 pervoskites," *Solid State Commun.*, vol. 149, no. 33–34, pp. 1359–1362, Sep. 2009.

[10] K. S. Aleksandrov and V. V. Beznosikov, "Hierarchies of pervoskite-like crystals (Review)," *Phys. Solid State*, vol. 39, no. 5, pp. 695–715, May 1997.

[11] S. N. Ruddlesden and P. Popper, "The compound Sr 3 Ti 2 O 7 and its structure," *Acta Crystallogr.*, vol. 11, no. 1, pp. 54–55, Jan. 1958.

[12] B. V. Beznosikov and K. S. Aleksandrov, "Pervoskite-like crystals of the Ruddlesden-Popper series," *Crystallogr. Reports*, vol. 45, no. 5, pp. 792–798, Sep.

2000.

[13] S. N. Ruddlesden and P. Popper, “New compounds of the K 2 NIF 4 type,” *Acta Crystallogr.*, vol. 10, no. 8, pp. 538–539, Aug. 1957.

[14] A. M. Glazer, “Simple ways of determining pervoskite structures,” *Acta Crystallogr. Sect. A*, vol. 31, no. 6, pp. 756–762, Nov. 1975.

[15] H. A. Jahn and E. Teller, “Stability of polyatomic molecules in degenerate electronic states - I—Orbital degeneracy,” *Proc. R. Soc. London. Ser. A - Math. Phys. Sci.*, vol. 161, no. 905, pp. 220–235, Jul. 1937.

[16] M. W. Lufaso and P. M. Woodward, “Jahn–Teller distortions, cation ordering and octahedral tilting in pervoskites,” *Acta Crystallogr. Sect. B Struct. Sci.*, vol. 60, no. 1, pp. 10–20, Feb. 2004.

[17] K. Yamakawa *et al.*, “Novel Pb(Ti, Zr)O 3 (PZT) Crystallization Technique Using Flash Lamp for Ferroelectric RAM (FeRAM) Embedded LSIs and One Transistor Type FeRAM Devices,” *Jpn. J. Appl. Phys.*, vol. 41, no. Part 1, No. 4B, pp. 2630–2634, Apr. 2002.

[18] D. W. Murphy *et al.*, “New superconducting cuprate pervoskites,” *Phys. Rev. Lett.*, vol. 58, no. 18, pp. 1888–1890, May 1987.

[19] S. Mitani *et al.*, “Tunnel-MR and spin electronics in metal–nonmetal granular systems,” *J. Magn. Magn. Mater.*, vol. 198–199, pp. 179–184, Jun. 1999.

[20] J. Druce, H. Téllez, T. Ishihara, and J. A. Kilner, “Oxygen exchange and transport in dual phase ceramic composite electrodes,” *Faraday Discuss.*, vol. 182, pp. 271–288, 2015.

[21] C. Suryanarayana and M. G. Norton, *X-Ray Diffraction*, 1st ed. Boston, MA: Springer US, 1998.

[22] V. M. Goldschmidt, “Die Gesetze der Krystallochemie,” *Naturwissenschaften*, vol. 14, no. 21, pp. 477–485, 1926.

[23] R. D. Shannon, “Revised effective ionic radii and systematic studies of interatomic distances in halides and chalcogenides,” *Acta Crystallogr. Sect. A*, vol. 32, no. 5, pp. 751–767, Sep. 1976.

[24] M. W. Lufaso and P. M. Woodward, “Prediction of the crystal structures of pervoskites using the software program SPuDS,” *Acta Crystallogr. Sect. B*, vol. 57, no. 6, pp. 725–738, 2001.

[25] D. Balzar and H. Ledbetter, "Voigt-function modeling in Fourier analysis of size- and strain-broadened X-ray diffraction peaks," *J. Appl. Crystallogr.*, vol. 26, no. 1, pp. 97–103, Feb. 1993.

[26] R. Jacob and I. Jayakumari, "X-ray diffraction line profile analysis of Ba Sr0.6 Fe0.4 TiO3 (BSFTO)," *Int. J. Chem. Stud.*, vol. 5, no. 2, pp. 12–21, 2015.

[27] W. H. Hall, "X-Ray Line Broadening in Metals," *Proc. Phys. Soc. Sect. A*, vol. 62, no. 11, pp. 741–743, Nov. 1949.

[28] B. E. Warren and B. L. Averbach, "The Separation of Cold-Work Distortion and Particle Size Broadening in X-Ray Patterns," *J. Appl. Phys.*, vol. 23, no. 4, pp. 497–497, Apr. 1952.

[29] M. Licheron, F. Gervais, J. Coutures, and J. Choisnet, "'Ba2BiO4' surprisingly found as a cubic double pervoskite," *Solid State Commun.*, vol. 75, no. 9, pp. 759–763, Sep. 1990.

[30] A. E. Lavat and E. J. Baran, "IR-spectroscopic characterization of A 2 BB 0 O 6 pervoskites," vol. 32, pp. 167–174, 2003.

[31] M. L. Craus, I. Rusu, and A. Rusu, "ON SOME MIXED OXIDES IN THE SYSTEM CaO-CdO-Bi 2 O 3 -Nb 2 O 5 . CATION DISTRIBUTION IN A DISTORTED AURIVILLIUS STRUCTURE − I calc obs calc," vol. 5, no. 3, pp. 653–656, 2003.

[32] C. N. R. Rao and J. Gopalakrishnan, *New Directions in Solid State Chemistry*. Cambridge University Press, 1997.

[33] F. Galasso and L. Katz, "Preparation and structure of Ba 5 Ta 4 O 15 and related compounds," *Acta Crystallogr.*, vol. 14, no. 6, pp. 647–650, Jun. 1961.

[34] R. Ratheesh, H. Sreemoolanadhan, and M. T. Sebastian, "Vibrational Analysis of Ba5−xSrxNb4O15Microwave Dielectric Ceramic Resonators," *J. Solid State Chem.*, vol. 131, no. 1, pp. 2–8, Jun. 1997.

[35] R. K. Tamrakar, D. P. Bisen, C. S. Robinson, I. P. Sahu, and N. Brahme, "Ytterbium Doped Gadolinium Oxide (Gd 2 O 3 :Yb 3+) Phosphor: Topology, Morphology, and Luminescence Behaviour," *Indian J. Mater. Sci.*, vol. 2014, pp. 1–7, 2014.

[36] R. K. Tamrakar, D. P. Bisen, and N. Brahme, "Comparison of photoluminescence properties of Gd 2 O 3 phosphor synthesized by combustion and solid state

reaction method," *J. Radiat. Res. Appl. Sci.*, vol. 7, no. 4, pp. 550–559, Oct. 2014.

[37] A. García-Murillo *et al.*, "Elaboration and scintillation properties of Eu3+-doped Gd2O3 and Lu2O3 sol–gel films," *Nucl. Instruments Methods Phys. Res. Sect. A Accel. Spectrometers, Detect. Assoc. Equip.*, vol. 486, no. 1–2, pp. 181–185, Jun. 2002.

[38] U. Balachandran and N. G. Eror, "Raman spectrum of the high temperature form of Nb2O5," *J. Mater. Sci. Lett.*, vol. 1, no. 9, pp. 374–376, Sep. 1982.

[39] A. E. L. Jazouli, C. Parent, G. L. E. Flem, and P. Hagenmuller, "Na4Nb (P04j3 , a Material with a Reversible Crystal-Glass Transformation : Structural and Optical Comparison," vol. 384, pp. 377–384, 1988.

[40] A. F. Corsmit, H. E. Hoefdraad, and G. Blasse, "Vibrational spectra of ordered pervoskites," *J. Inorg. Nucl. Chem.*, vol. 34, no. 11, pp. 3401–3404, Nov. 1972.

[41] G. Blasse and A. F. Corsmit, "Electronic and vibrational spectra of ordered pervoskites," *J. Solid State Chem.*, vol. 6, no. 4, pp. 513–518, Apr. 1973.

[42] A. Dutta and T. P. Sinha, "Dielectric Relaxation and Electronic Structure of Double Pervoskite Ca2AlNbO6," *Integr. Ferroelectr.*, vol. 116, no. July 2015, pp. 41–50, 2010.

[43] G. Blasse and B. C. Grabmaier, *Luminescent Materials*. Berlin, Heidelberg: Springer Berlin Heidelberg, 1994.

[44] P. Ptacek, H. Schäfer, K. Kömpe, and M. Haase, "Crystal Phase Control of Luminescing α-NaGdF4:Eu3+and β-NaGdF4:Eu3+ Nanocrystals," *Adv. Funct. Mater.*, vol. 17, no. 18, pp. 3843–3848, Dec. 2007.

[45] Y.-H. Won, H. S. Jang, W. Bin Im, and D. Y. Jeon, "Red-Emitting LiLa2O2BO3:Sm3+,Eu3+ Phosphor for Near-Ultraviolet Light-Emitting Diodes-Based Solid-State Lighting," *J. Electrochem. Soc.*, vol. 155, no. 9, p. J226, 2008.

[46] K. V. Dabre, K. Park, and S. J. Dhoble, "Synthesis and photoluminescence properties of microcrystalline Sr 2 ZnWO 6 :RE 3+ (RE = Eu, Dy, Sm and Pr) phosphors," *J. Alloys Compd.*, vol. 617, pp. 129–134, Dec. 2014.

[47] F. M. Emen and R. Altinkaya, "Luminescence and thermoluminescence properties of Sr3WO6:Eu3+ phosphor," *J. Lumin.*, vol. 134, pp. 618–621, Feb. 2013.

[48] S. Zhang, Y. Hu, L. Chen, X. Wang, G. Ju, and Y. Fan, "Photoluminescence properties of Ca3WO6:Eu3+ red phosphor," *J. Lumin.*, vol. 142, pp. 116–121,

Oct. 2013.

[49] W. F. Zhang, Z. Yin, M. S. Zhang, Z. L. Du, and W. C. Chen, "Roles of defects and grain sizes in photoluminescence of nanocrystalline SrTiO 3," *J. Phys. Condens. Matter*, vol. 11, no. 29, pp. 5655–5660, Jul. 1999.

[50] X. Zhao, Y. Ding, Z. Li, T. Yu, and Z. Zou, "An efficient charge compensated red phosphor Sr3WO6: K+, Eu3+ – For white LEDs," *J. Alloys Compd.*, vol. 553, pp. 221–224, Mar. 2013.

[51] X. Zhao *et al.*, "Efficient red phosphor double-pervoskite Ca3WO6 with A-site substitution of Eu3+," *Dalt. Trans.*, vol. 42, no. 37, p. 13502, 2013.

[52] N. Jain *et al.*, "Synthesis and Rational design of Europium and Lithium Doped Sodium Zinc Molybdate with Red Emission for Optical Imaging," *Sci. Rep.*, vol. 9, no. 1, p. 2472, Dec. 2019.

[53] Y. Gao *et al.*, "Tb 3+ and Eu 3+ co-doped Ba 6 Bi 9 B 79 O 138 : color-tunable phosphors by utilizing the host-sensitization effect of Bi 3+ and enhancement of red emission upon heating," *New J. Chem.*, vol. 41, no. 5, pp. 2037–2045, 2017.

[54] A. Katelnikovas, H. Winkler, A. Kareiva, and T. Jüstel, "Synthesis and optical properties of green to orange tunable garnet phosphors for pcLEDs," *Opt. Mater. (Amst).*, vol. 33, no. 7, pp. 992–995, May 2011.

[55] D. Chen, Y. Wang, Y. Yu, P. Huang, and F. Weng, "Novel rare earth ions-doped oxyfluoride nano-composite with efficient upconversion white-light emission," *J. Solid State Chem.*, vol. 181, no. 10, pp. 2763–2767, Oct. 2008.

[56] J. S. Zhong, H. B. Gao, Y. J. Yuan, L. F. Chen, D. Q. Chen, and Z. G. Ji, "Eu3+-doped double pervoskite-based phosphor-in-glass color converter for high-power warm w-LEDs," *J. Alloys Compd.*, vol. 735, pp. 2303–2310, Feb. 2018.

[57] Y. Bai, T. Siponkoski, J. Peräntie, H. Jantunen, and J. Juuti, "Ferroelectric, pyroelectric, and piezoelectric properties of a photovoltaic pervoskite oxide," *Appl. Phys. Lett.*, vol. 110, no. 6, p. 063903, Feb. 2017.

[58] J. Zheng, Q. Cheng, C. Zheng, G. Chen, F. Shi, and C. Chen, "Correlated color temperature tunability and energy transfer phenomenon in the NaBaBO 3 : Dy 3+ / Eu 3+ phosphor for white light application," *Funct. Mater. Lett.*, vol. 08, no. 06, p. 1550077, Dec. 2015.